Optical control of a dark exciton reservoir

A. S. Kurdyubov,[1,*] A. V. Trifonov,[1,2] I. Ya. Gerlovin,[1] B. F. Gribakin,[1] P. S. Grigoryev,[1] A. V. Mikhailov,[1] I. V. Ignatiev,[1] Yu. P. Efimov,[3] S. A. Eliseev,[3] V. A. Lovtcius,[3] M. Aßmann,[2] M. Bayer,[2] and A. V. Kavokin[4,5,1]

[1]*Spin Optics Laboratory, St. Petersburg State University, Ulyanovskaya 1, Peterhof, St. Petersburg 198504, Russia*

[2]*Experimentelle Physik 2, Technische Universität Dortmund, 44221 Dortmund, Germany*

[3]*Resource Center "Nanophotonics", St. Petersburg State University, Ulyanovskaya 1, Peterhof, St. Petersburg 198504, Russia*

[4]*Westlake University, School of Science, 18 Shilongshan Road, Hangzhou 310024, Zhejiang Province, China*

[5]*Westlake Institute for Advanced Study, Institute of Natural Sciences, 18 Shilongshan Road, Hangzhou 310024, Zhejiang Province, China*

(Received 21 April 2021; revised 15 June 2021; accepted 17 June 2021; published 12 July 2021)

Optically inactive or dark excitons play an important role in exciton and polariton devices. On one hand, they supply excitons to the light cone and feed the photoluminescence signal. On the other hand, they repel radiatively active excitons due to the exchange interaction and contribute to the formation of lateral potentials for exciton and polariton condensates. On top of this, they play an important role in scattering and energy relaxation dynamics of quasiparticles in semiconductors. So far, because of optical inaccessibility, studies were focused typically on one experimental technique, giving information about one quantity of dark excitons. Here we present a comprehensive study of the dark exciton reservoir in a high-quality 14-nm GaAs/AlGaAs quantum well using several experimental techniques. We develop a new method of nonradiative broadening spectroscopy of exciton resonances and combine it with nondegenerate pump-probe spectroscopy. The exciton and carrier dynamics in the reservoir is monitored via dynamic broadening of exciton resonances induced by exciton-exciton and exciton-carrier scattering. The dynamics is found to be strongly dependent on the optical excitation conditions. Based on the experimental results, we develop a model of dynamics in a reservoir of excitons and free carriers. The model allows us to describe the experimentally measured photoluminescence kinetics with no fitting parameters. We also demonstrate the optical control of the dark exciton density by means of an additional excitation that creates imbalance of free carriers depleting the reservoir. These results shed light onto the dynamics of the excitonic "dark matter" and pave the way to the high-precision engineering of optically induced potentials in exciton-polariton and integrated photonic devices. We expect that the observed results can be transferred also to other semiconductors so that the current quantum well serves as a high-quality model system.

DOI: 10.1103/PhysRevB.104.035414

I. INTRODUCTION

Excitons dominate the low-temperature optical spectra of semiconductors [1–4]. These quasiparticles play a crucial role in a number of remarkable fundamental effects such as the Bose-Einstein condensation and superfluidity, polariton lasing, spin Hall effect, etc. [5–11]. Experimentally, mostly the bright excitons that efficiently couple to light have been studied until now. The typical bright exciton radiative recombination time in a semiconductor quantum well (QW) is on the order of units or tens of picoseconds [3,12,13]. In contrast, the exciton photoluminescence (PL) kinetics in QWs under pulsed non-resonant excitation typically decays in 1 ns [14]. This drastic difference illustrates that PL kinetics directly depend on the relaxation processes preceding the formation of radiative (bright) excitons.

In these relaxation processes, an important role is attributed to the photocreated free carriers and hot excitons with a large wave vector K_X of propagation along the QW layer (the in-plane wave vector) exceeding the wave vector of light K_c in the QW material. Such excitons cannot recombine with photon emission because of the wave-vector selection rule. This is why they are frequently referred to as nonradiative or "dark" excitons. Excitons with angular momentum $J = 2$ which cannot emit light because of the spin selection rules also contribute to the reservoir of dark excitons. Note that in GaAs-based quantum wells, the splitting between excitons with $J = 1$ and 2 is less than 0.1 meV [15]. Even at a temperature of 1 K, such excitons are in equilibrium. The phonon bottleneck effect [16,17] leads to slow relaxation of the nonradiative excitons towards radiative states with $K_X < K_c$. Thus, the excitons not interacting with light are decoupled from other subsystems allowing one to introduce the concept of an exciton reservoir, which can live for tens of ns in high-quality structures [18].

The areal density of the nonradiative excitons can exceed that of the radiative ones by orders of magnitude in the steady-state experiments. Although the reservoir of nonradiative excitons is a "dark matter," which cannot be directly tested by light, it is feasible to test its effect on the radiative excitons. In particular, the exciton lines in optical spectra can considerably broaden because of the scattering of the radiative and nonradiative excitons [19].

In a general case, the reservoir consists of a mixture of nonradiative excitons and free carriers [20,21]. Many fundamental processes determine the dynamics of this system.

*kurdyubov@yandex.ru

 ©2021 American Physical Society

These include exciton and carrier energy relaxation and thermalization, the coupling of electrons and holes into excitons, dissociation of excitons at elevated temperatures, and the scattering of excitons from the reservoir into the light cone followed by fast recombination. The rate of these processes strongly depends on the experimental conditions, such as the photon energy of the excitation, its power density, or the sample temperature. There have been many attempts to study these processes experimentally and theoretically.

Up to now, experimental approaches have focused on two main methods: the first one relies on the PL kinetics [14,22–30]. However, using this approach, excitons in the reservoir may be studied only indirectly because the PL appears only after the excitons have already scattered from the reservoir into the light cone.

The second, more direct method, deals with terahertz (THz) experiments [26,31–37]. The transition between $1s$ and $2p$ exciton states typically falls into the THz range. Therefore, the resonant absorption at the corresponding frequency in the range from 1 to 2 THz depending on the QW width allows one to estimate the exciton density. It is worth noting here that it has always been a big problem to assess the exciton density quantitatively, already for the bright, but also for the dark excitons. Nonresonant THz absorption is also a viable tool to estimate the carrier density in the electron-hole plasma. In a two-color pump-probe setting, a near-infrared pump beam and a THz probe beam may be applied to study the exciton and carrier dynamics in the reservoir. The main drawback of this method is its relatively low sensitivity, related to the small cross section of the THz absorption. Therefore, these experiments require pump pulses with relatively large powers, which considerably affect the exciton and carrier dynamics in the reservoir.

Recently, a new approach of tracking dark excitons in the reservoir with exciton polaritons was suggested [10]. Using polariton bistability, authors found the long-lived ($>$20 ns) exciton reservoir in microcavity exciton-polariton systems. However, this experimental approach only works in microcavity systems.

Accordingly, the theoretical modeling of the excitonic reservoir behavior is challenging as it may only rely on the scarce experimental data available. First attempts of such modeling [38–40] provoked an extensive and contradictory discussion of the primary mechanisms of the formation of the exciton PL signal [25–28,30,34,36,41,42]. The widely used model assumes the formation of excitons in the reservoir by photoexcited electrons and holes. When formed, these excitons are scattered by other excitons or acoustic phonons into the light cone, where they recombine by emitting light. Both processes, namely, the exciton formation and their scattering to the light cone, are slow compared to the exciton radiative recombination because they involve interactions with acoustic phonons. The scattering to the light cone slows down also due to a small number of available quantum states for excitons within the light cone, as compared to the number of quantum states in the reservoir. At low excitation powers and temperatures, these considerations are sufficient to explain the slow rise and decay of the exciton PL moderately well. However, the complex time dependence of the PL signal at increased excitation powers and/or elevated temperatures requires a more sophisticated theory. In particular, one observes a shortening of the rise and decay times of the PL signal, which requires new theoretical considerations.

In Ref. [40] an explanation for the shortening of the PL rise time is proposed. The authors suggest that the recombination of Coulomb-correlated electron-hole pairs is responsible for the PL signal at the exciton resonance frequency rather than true excitonic recombination. This idea has been tested experimentally in many works [25–28,30,34,36]. However, there is still no general consensus with respect to this question. The reasons for the persisting ambiguity regarding the origin of the exciton PL signal are (1) the number of processes involved in the PL signal dynamics is large, (2) the rates of these processes are sensitive to the particular experimental conditions, (3) the experimental data are not sufficient to draw unambiguous conclusions about each of the processes involved.

As one can see from the discussion above, the available knowledge about the physical processes occurring in the reservoir and their dependence on external conditions is limited. Moreover, the available experimental data were obtained on structures of different quality. Composition, size fluctuations, and other defects in the QW structure under study can significantly impact experiments giving rise to false conclusions.

In this work, we investigate the exciton-carrier reservoir considering various methods of its photocreation and various channels of signal detection. We study a high-quality heterostructure with a 14-nm shallow $GaAs/Al_{0.03}Ga_{0.97}As$ QW, in which only fundamental processes control the exciton-carrier dynamics in the reservoir. To get the complete information about the processes in the reservoir, we used the spectrally resolved pump-probe technique described in Ref. [15]. Here, the main quantity of interest is the dynamics of the nonradiative broadening of exciton resonances [15,43]. This technique allows instantaneous access to the exciton and carrier concentrations in the reservoir, thus enabling the study of their dynamics. To distinguish between the contributions of the reservoir excitons and free carriers, we measure the broadening dynamics at several optical excitation energies. We found that in cases where both excitons and free carriers are created in the QW, the excitons in the nonradiative reservoir survive up to the next laser pulse. In other words, their lifetime exceeds 12.5 ns. The small depth of potential wells in the QW structure under study allowed us to selectively implement excitation conditions for which either electrons, or holes, or both types of carriers are created in the barrier layers. We found the exciton reservoir to efficiently deplete in case of imbalance in the photocreated electrons and holes in the QW. This indicates the key role of exciton-carrier scattering in the depletion of the reservoir.

The paper is organized as follows. In the first two sections, we explain the employed method by which we measure the excitation spectra of the nonradiative broadening of exciton resonances. Using it and the PL excitation (PLE) spectra, we suggest a model of the energy structure of the exciton and carrier states in our sample (see Sec. IV). This model provides a reasonable choice of experimental conditions to study the reservoir dynamics. We describe this dynamics study in Sec. V. The next section describes the model for the dynamics, which we develop to explain the experimental observations. The model, in particular, predicts the PL signal profiles for

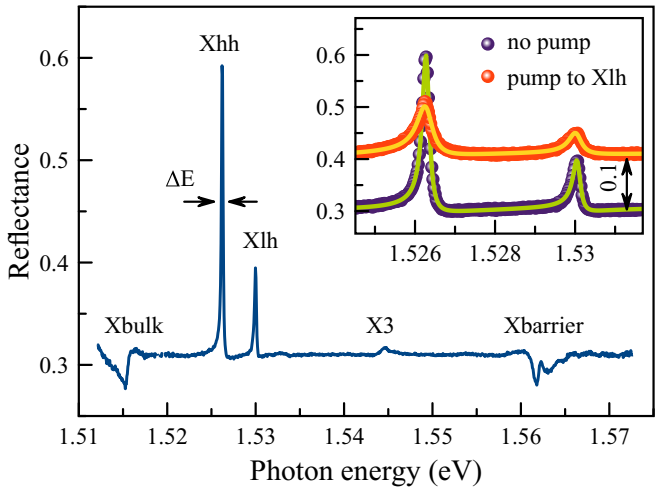

FIG. 1. The reflectivity spectrum of the studied QW structure measured at $T = 5$ K. Labels Xhh and Xlh mark the ground states of the heavy-hole and light-hole excitons in the QW. Resonance "X3" can be tentatively ascribed to the third quantum-confined state of the heavy-hole exciton. Inset shows fragments of the reflectivity spectra measured with no pump (lower curve) and in the presence of an additional cw excitation of the power density $P_{cw} = 1$ W/cm^2 resonant with the Xlh exciton transition (upper curve). The upper spectrum is vertically shifted by 0.1 for the clarity of presentation. Solid lines show the fits using Eqs. (1) and (2).

all excitation conditions. We compare these predictions with experimentally measured PL kinetics in Sec. VII. Section VIII discusses the obtained experimental results and their modeling. Then, we demonstrate a possibility to control the exciton reservoir in Sec. IX. Finally, we summarize our findings in the Conclusion.

II. REFLECTIVITY SPECTRA

The structure under study was grown by molecular beam epitaxy (MBE) on n-doped (001) GaAs substrate. The sample contains a 14-nm GaAs QW layer sandwiched between $Al_xGa_{1-x}As$ barrier layers with $x \approx 3\%$. Such low aluminum content maintains a high structural quality of samples, possibly suppressing the built-in deformations [44]. Shallow, a few tens of meV, potential wells allow one to study the energy structure of excitonic and carrier states in the whole energy range from the lowest heavy-hole exciton state in the QW up to the bulk exciton state in the barrier layers.

We measured reflectivity spectra of the structure at normal incidence of a probe laser beam. Spectrally broad 80-fs pulses of a Ti:sapphire laser, used in these experiments, cover the whole spectral range studied. The reflected laser beam was dispersed in a 0.5-m spectrometer with an 1800 gr/mm grating and detected by a nitrogen-cooled CCD array. The detected signal was normalized with respect to the laser spectral profile to obtain the reflectivity spectra of the sample.

A typical reflectivity spectrum of the studied QW structure is shown in Fig. 1. It displays the heavy-hole (Xhh) and light-hole (Xlh) exciton resonances in the spectral region of 1.525–1.535 meV. The resonances appear as peaks due to the intentional choice of the top sample layer thickness. The spectrum also displays features related to the excitons in the thick GaAs buffer layer and in the AlGaAs barrier layers. The energy gap between these features provides a good estimate for the joint depth of potential wells for carriers of about 46 meV.

The inset in Fig. 1 shows a fragment of the reflectivity spectra in the spectral vicinity of Xhh and Xlh resonances. The spectral widths of the resonances are very sensitive to the excitation conditions. In the regime of a weak probe beam intensity of 1 μW per spot area of 10^4 μm^2 with no additional illumination applied, the full width at a half-maximum of the Xhh resonance is only $\Delta E = 185$ μeV. Such a small spectral width of the exciton resonance indicates the high quality of the sample. With additional illumination by a continuous-wave (cw) laser, the resonances broaden (see the upper spectrum in the inset). The cw excitation creates excitons and/or free carriers. The photocreated quasiparticles interact with bright excitons leading to resonance broadening. Therefore, the broadening provides information on the interaction in certain experimental conditions, and we use it as the main method of study in our work.

The exciton resonances can be modeled in the framework of the nonlocal optical response theory described in Ref. [4] which has been applied to the analysis of experimental data in many works (see, e.g., Refs. [13,15,18,44–46]). The amplitude reflection coefficient of a QW, $r_{QW}(\omega)$, in the vicinity of frequency ω_X of a single exciton resonance is given by the expression

$$r_{QW}(\omega) = \frac{i\Gamma_R}{\omega_X - \omega - i(\Gamma_R + \Gamma_{NR})}, \tag{1}$$

where Γ_R and Γ_{NR} are the radiative and nonradiative exciton relaxation rates, respectively. The total intensity of the reflected light depends also on the amplitude reflection coefficient of the sample surface r_s and can be expressed as

$$R(\omega) = \left| \frac{r_s + r_{QW}(\omega)e^{i2\phi}}{1 + r_s r_{QW}(\omega)e^{i2\phi}} \right|^2, \tag{2}$$

where ϕ is the phase acquired by the light wave propagating through the top layer of the structure to the middle of the QW layer.

Equations (1) and (2) are used to fit the spectra shown in the inset of Fig. 1. One can see that the calculated curves perfectly reproduce all peculiarities of the resonances. In particular, they describe the Lorentz-type profile of the resonances with slowly decaying wings. This proves that there is no noticeable inhomogeneous broadening in the exciton system. Such broadening would result in Gaussian-type wings with a faster decay than the observed Lorentzian wings.

Perfect agreement of the experimental and calculated curves allows one to reliably extract the main parameters of exciton resonances, namely, the radiative ($\hbar\Gamma_R$) and nonradiative ($\hbar\Gamma_{NR}$) broadenings as well as the exciton energy ($\hbar\omega_X$) with accuracy from few μeV to fractions of μeV. Of course, some systematic errors in the obtained values are also possible.

The homogeneous nonradiative broadening of exciton resonances $\hbar\Gamma_{NR}$ is caused by the interaction (scattering processes) of bright excitons with other quasiparticles in the

system, such as phonons, excitons, and free carriers [18,44]. The effect of quasiparticles created by a cw illumination of the sample to the Xlh resonance is shown in the inset in Fig. 1. Interactions with these quasiparticles increase the nonradiative broadening of the Xhh resonance from 42 up to 194 μeV at the relatively small cw excitation power of 0.75 mW per laser spot $S_{cw} \approx 10^4$ μm^2. The high sensitivity of the nonradiative broadening to the scattering processes allows one to study in detail the energy spectrum of the quasiparticles involved and the dynamics of the scattering processes.

III. NBE SPECTRA

To study the nonradiative broadening, we excited the sample by a tunable cw laser focused onto the same point as the femtosecond probe beam. We tuned the energy of the cw laser, $\hbar\omega_{cw}$, in order to study the photoexcitation spectral dependencies of various characteristics of exciton resonances. The excitation power was stabilized at a certain fixed value, P_{cw}, controlled by a variable attenuator with a built-in "noise eater" feedback feature. We measured the reflectivity spectra, as its is described above, for each particular energy $\hbar\omega_{cw}$, and fitted them using Eqs. (1) and (2). As a result, we obtained the dependencies of all parameters of each exciton resonance on $\hbar\omega_{cw}$.

Figure 2(a) shows an example of the variable part of the obtained dependencies of the nonradiative broadening $\hbar\Gamma_{NR}(\hbar\omega_{cw})$, for the Xhh and Xlh resonances. Hereafter, they will be referred to as the nonradiative broadening excitation (NBE) spectra. The NBE spectra demonstrate rich spectral structures, more pronounced than those of the reflectivity spectra shown in Fig. 1. In particular, in the NBE spectrum, peaks of $\hbar\Gamma_{NR}$ are observed at the Xhh and Xlh resonances, also seen in the reflectance spectrum. Besides, a steplike increase of the broadening, an additional peak X3, and a dip are present in the range of 1.53–1.56 eV. These features are absent in the reflectivity spectrum.

The NBE spectrum of the Xlh resonance is similar to that of the Xhh resonance. The amplitude in the spectral range 1.525–1.552 eV, however, is smaller compared to that of the Xhh resonance. Figure 2(a) shows a comparison of the variable parts of the resonances' broadening, $\Delta\hbar\Gamma_{NR} = \hbar\Gamma_{NR} - \hbar\Gamma_{NR}^{(0)}$, where $\hbar\Gamma_{NR}^{(0)}$ is the broadening measured with no cw pumping: $\hbar\Gamma_{NR}^{(0)} = 42$ μeV for the Xhh resonance and $\hbar\Gamma_{NR}^{(0)} = 79$ μeV for the Xlh resonance. The larger value of $\hbar\Gamma_{NR}^{(0)}$ for the Xlh resonance most likely originates from the exciton relaxation from the Xlh to the Xhh state.

Analyzing the data in Fig. 2(a), we draw several valuable conclusions. Features in the NBE spectrum come from the absorption of cw radiation, generating excitons and/or free carriers. Excitons generated in the resonant absorption regime at the Xhh and Xlh transitions can recombine and emit photons. There exists, however, a competing relaxation process. In particular, excitons may be redistributed to states outside the light cone and populate a reservoir of nonradiative excitons with large in-plane wave vectors [18]. This process is illustrated in Fig. 2(b). The Xlh excitons may scatter to the reservoir by emitting acoustic phonons, which is possible even at zero temperature.

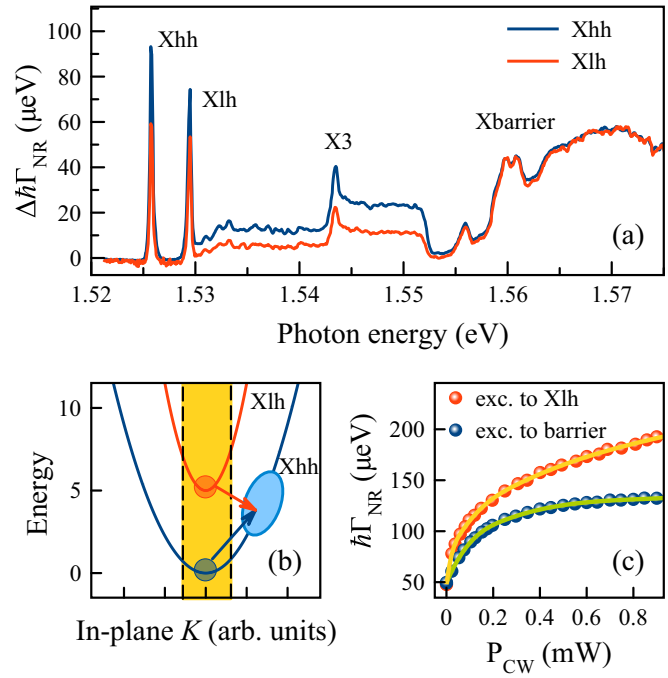

FIG. 2. (a) Comparison of the variable part of the NBE spectra for the Xhh (blue curve) and Xlh (red curve) exciton resonances. The background broadening not related to the optical excitation is subtracted: 42 μeV for the Xhh and 79 μeV for the Xlh. $P_{cw} = 0.15$ mW. (b) Schematic representation of the population of the nonradiative reservoir. The parabolas show the Xhh and Xlh exciton energies as functions of the in-plane wave vector K_x or K_y. The yellow area is the light cone and the light blue oval is the nonradiative reservoir. Arrows show the ejection processes. (c) cw pump-power dependencies of the nonradiative broadening of the Xhh resonance under cw excitation to the Xlh resonance ($E_{cw} = 1.530$ eV) and to the barriers ($E_{cw} = 1.570$ eV). Solid lines are the guides for the eye.

Xhh excitons need to absorb phonons to reach states in the reservoir, which requires nonzero lattice temperature. However, the critical kinetic energy for such processes is small, $E_c = (\hbar^2 K_c^2)/(2M_{xy}) \approx 0.17$ meV. Here $M_{xy} = m_0(m_e^* + m_{hhxy}^*) = 0.177\, m_0$ is the in-plane exciton mass [47], K_c is the wave vector corresponding to the edge of the light cone, $K_c = 2\pi/(\lambda/n) \approx 2.8 \times 10^5$ cm^{-1}, where $n = 3.6$ is the refractive index of GaAs. The critical energy E_c corresponds to the sample temperature $T \approx 2$ K. So, phonon-assisted scattering of excitons to the reservoir is possible at the temperatures $T \approx 5$ K used in our experiments.

The efficiency of exciton transfer towards the reservoir depends on the ratio of the phonon scattering and radiative recombination rates. It is higher for Xlh excitons than for Xhh excitons because of the slower radiative decay and the additional contribution of phonon emission processes in the case of Xlh excitons. Consequently, exciton reservoir becomes populated faster when exciting the Xlh resonance rather than the Xhh resonance. That is why the Xhh and Xlh nonradiative broadening peaks in Fig. 2(a) have almost the same amplitudes, in contrast to the peaks in the reflectivity spectrum (compare to Fig. 1).

Due to the long lifetime of the nonradiative excitons, the reservoir can accumulate a large number of excitons. These

are the quasiparticles mainly responsible for the broadening of exciton resonances in the reflectivity spectra at these excitation conditions. The reservoir excitons have enough time to reach thermal equilibrium with the crystal lattice [48]. At the low $T < 10$ K, used in most experiments, the kinetic energy of the excitons, $E_{\text{kin}} = kT < 1$ meV, that is smaller than the energy gap between the Xlh and Xhh exciton energies, $\delta E \approx 3.8$ meV (see inset in Fig. 1). Therefore, the majority of excitons in the reservoir are the heavy-hole excitons.

A theoretical analysis shows [49] that the main mechanism of interaction of the reservoir excitons with the radiative excitons is the exchange interaction. The strength of the interaction of Xhh reservoir excitons with Xhh radiative excitons (the Xhh-Xhh interaction) is composed of almost equal contributions of the electron-electron exchange interaction $S_{\text{e-e}}$, and the hole-hole exchange interaction $S_{\text{hh-hh}}$. The similar exchange interaction of Xhh excitons with Xlh radiative excitons (the Xhh-Xlh interaction) is approximately twice smaller because the heavy-hole–light-hole exchange $S_{\text{hh-lh}}$ is suppressed. Therefore, we should expect that the photoinduced broadening of the Xlh resonance should be twice as small as that of the Xhh resonance. Experimental data presented in Fig. 2(a) qualitatively confirm this conclusion. Indeed, the experimental ratio R of the Xhh and Xlh NBE amplitudes [blue and red curves in Fig. 2(a)] in the spectral region $\Delta E =$ 1.530–1.552 eV is nearly two, $R \approx 1.9$. For the Xhh and Xlh peaks, this ratio is slightly less, $R \approx 1.6$.

Interestingly, R remains close to 2 in a wide spectral range up to the "dip" at 1.552 eV, including the spectral region where free carriers are generated in addition to excitons. In the higher-energy region, the NBE spectra for the Xhh and Xlh resonances almost coincide. The observed pronounced difference in the NBE spectra in these two spectral regions indicates that the dynamics of quasiparticles differ in these regions. We discuss this in the next section.

Figure 2(c) shows the cw pump-power dependence of the Xhh resonance broadening under excitation to the Xlh and barrier optical transitions. The observed sublinear dependencies are characteristic features of the complex dynamics of the exciton-free carrier reservoir discussed in Sec. VI. Another possible contribution to the observed sublinearity is related to the decrease of the absorption coefficient once the nonradiative broadening of this resonance increases [4,50].

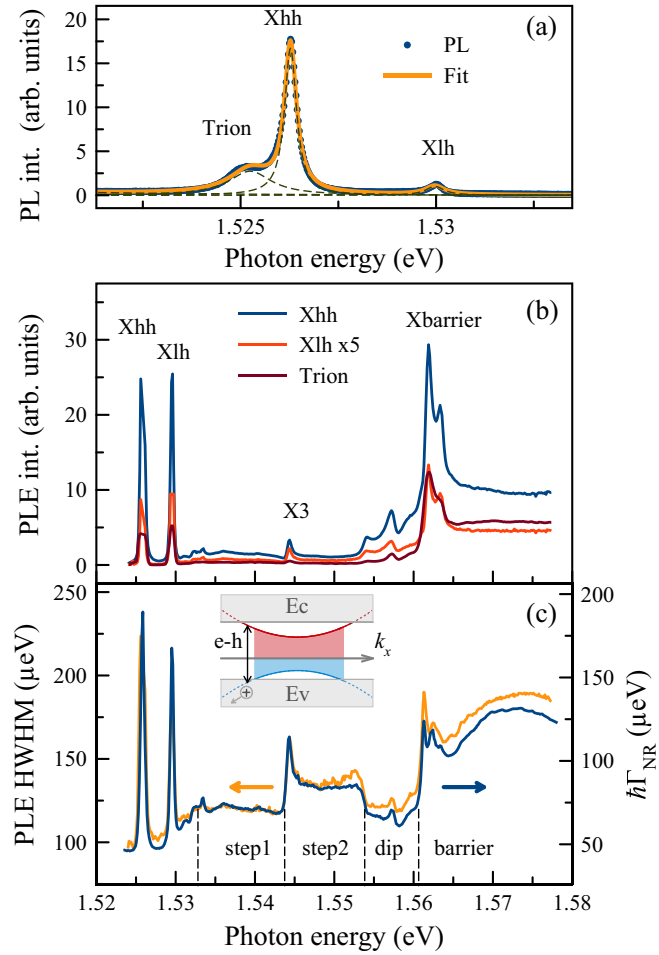

FIG. 3. (a) An example of the PL spectrum measured for excitation to the barrier layer optical transitions ($E_{\text{exc}} = 1.58$ eV, $P_{\text{exc}} =$ 0.78 mW). Solid curves show fits by the sum of Lorentzians (dashed curves). (b) PLE spectra of the Xhh, Xlh, and trion lines obtained as areas A_j under the respective Lorentz contours as functions of the photon energy of the cw excitation. The intensity of the Xlh line is multiplied by 5. (c) Comparison of the NBE spectrum (blue curve, right axis) and of the spectrum of HWHM (orange curve, left axis) for the Xhh exciton. The dashed vertical lines separate the spectral regions discussed in the text. The inset illustrates the mechanism of the "dip" spectral region formation.

IV. PLE SPECTRA

PLE spectra are typically used to study excited states of excitons and free carriers in heterostructures. We measured the PLE spectra on our setup, simply measuring the PL spectrum instead of the reflectivity at each excitation photon energy. An exemplary PL spectrum is shown in Fig. 3(a) by blue dots. The Xhh and Xlh exciton lines can be observed clearly and a third line shows up at the low-energy side of the Xhh line. Each spectral line can be accurately modeled by a Lorentz function

$$L(\omega) = \frac{A}{\pi\,\delta\omega[1 + (\omega_0 - \omega)^2/(\delta\omega)^2]},$$

where A is the area under the Lorentzian, ω_0 is the resonant frequency, and $\delta\omega$ is the half-width at half-maximum (HWHM) of the Lorentzian. Fitting the spectra by the sum of the Lorentzians, we extract the main parameters of the spectral lines. The low-energy spectral line can be tentatively ascribed to the trion transition shifted from the Xhh exciton by the binding energy $\delta E_T = 1.04 \pm 0.1$ meV. The trion line in fact can be a sum of spectral lines of the positively (X^+) and negatively (X^-) charged trions and may also contain a contribution of biexcitons. They all have almost the same binding energy.

The PLE spectra, i.e., the dependencies of the area A_j on the cw excitation energy for three PL lines, are shown in Fig. 3(b). The spectra contain several main peculiarities similar to those observed in the reflectivity spectrum (see Fig. 1).

However, in the "dip" spectral region (1.554–1.561 eV), PL intensity increases for all three PL lines, which contrasts with the decreasing amplitude observed in the NBE spectra [see Fig. 2(a)]. This means that the absorption coefficient in this spectral region has no dip. This intriguing result becomes even more contradictory if we consider the broadening of the PL lines.

The Xhh PL line broadening $\hbar\delta\omega_{\rm PL}$ depends on the excitation energy unlike the PL line area. Figure 3(c) compares this dependence for the Xhh exciton with the NBE spectrum. A remarkable similarity of the two spectra is obvious. In particular, a dip in the PL line is clearly seen and broadening coincides with that in the NBE spectrum.

The PL line broadening has an overall shift by a value of about 50 μeV relative to the NBE signal, as one can see comparing vertical axes in this figure. This shift must originate from the radiative broadening of the exciton resonance $\hbar\delta\omega_{\rm PL} \approx \hbar\Gamma_{\rm NR} + \hbar\Gamma_{\rm R}$.

We divide the spectra shown in Fig. 3(c) into several spectral regions marked "step1," "step2," "dip," and "barrier." The region "step1" evidently corresponds to optical transitions, hh1–e1, between the quantum-confined ground states for the electron (e1) and the heavy hole (hh1) with finite wave vectors along the QW layer. The density of states of quasi-two-dimensional (quasi-2D) carriers with parabolic dispersion is known to be constant [51], which explains the flatness of the spectra in this region. The lower edge of the step corresponds to an energy exactly one exciton Rydberg energy $R_x \approx 7$ meV above the Xhh exciton energy [13]. So, below the edge excitons will form, while above the edge free electrons and holes will form instead. Besides, there are Coulomb-correlated scattering states, which modifies the 2D density of states only slightly in QWs [45].

The interpretation of the "step2" plateau is more problematic because of the strong mixing of the hole states in QWs [52–54]. We believe that this spectral range is similar to "step1" and corresponds to optical transitions between the quantum-confined states of free electrons (e1) and mixed heavy-hole–light-hole states (hh2–lh1) in the QW. We tentatively ascribed the X3 peak to the third quantum-confined state of the Xhh exciton. The even wave function of this state provides stronger exciton-light coupling than the odd wave function of the second confined state [45].

The spectral region marked as "dip" in Fig. 3(c) is the most intriguing part of the spectra. On one hand, the dip in the line broadening seems to indicate a smaller number of photocreated excitons and carriers, which scatter with bright excitons. This could be ascribed to a decrease of the absorption coefficient in this region. On the other hand, the significant increase of the PL intensity in this spectral region observed in the PLE spectra in Fig. 3(b) indicates increased absorption.

We assume that the "dip" corresponds to optical transitions, which create carriers of a specific type, either electrons or holes, in the QW layer, while the other type is created in the barrier layers. Under these circumstances, nonradiative excitons cannot accumulate in the reservoir since the gas of electrons or holes efficiently scatters them into the light cone. Such an effect will be visible in time-resolved measurements, which we will focus on in the next section.

The inset in Fig. 3(c) shows a scheme of the optical transitions taking place for excitation to this region. The parabolic dispersion curves describe the carrier energies versus the in-plane carrier wave vector k_x. At certain values of $k_x = k^{\rm max}$, the carriers' energy exceeds V_c or V_v (the solid horizontal lines) corresponding to the edge of the conduction band or the valence band in the barriers. Such carriers can leave the QW and delocalize in the barrier layers. The delocalization first appears for one type of carriers, setting the left edge of the "dip" spectral region. The right edge appears when both types of carriers delocalize in the barrier layers.

The last spectral region marked in Fig. 3(c) as "barrier" is evidently formed by optical transitions where both the electron and hole states form in the barriers. The density of states in thick barriers far above Xbarrier grows as the square root of energy, dragging up the signal. A decrease in the signal at photon energies above 1.575 eV possibly comes from ever-increasing absorption concentrating the photocreated carriers near the sample surface, far from the QW layer.

V. PUMP-PROBE EXPERIMENTS

To study the exciton dynamics, we perform spectrally resolved pump-probe measurements. Our setup utilizes a femtosecond Ti:sapphire laser as a light source. The laser beam is split into a pump and a probe beam. The pump beam passes through an acousto-optic tunable filter forming spectrally narrow pulses of HWHM $\delta E_{\rm pump} \approx 0.48$ meV. It hits the sample perpendicularly to its surface and is focused onto a spot of about 95 μm in diameter. The delayed in time spectrally wide probe pulses ($\delta E_{\rm probe} \approx 45$ meV at 10% of the pulse maximum) are used to measure reflectivity spectra as described in Sec. II. We analyzed the measured spectra with the use of Eqs. (1) and (2).

Figure 4 shows examples of dependencies of the nonradiative broadening of the Xhh and Xlh resonances on the time delay τ between the pump and probe pulses. The laser excitation energy was centered at the Xlh transition. The dynamic curves measured for excitation at the Xhh transition demonstrate similar behavior. In Fig. 4, only the variable parts of the broadening $\Delta\hbar\Gamma_{\rm NR}$ induced by the pump pulses are shown. The dependencies measured at strong excitation power, $P = 2$ mW, consist of a very narrow initial part (pulse) with a duration of about several ps (see the inset in the figure) and a slowly varying signal. We ascribe the pulse to the interactions of radiative excitons before their radiative decay, which takes place on a 10-ps scale [13,18].

The slowly varying signal has rising and decaying parts. At weak excitation, the signal is well fitted by a two-exponential function with a background

$$f(\tau) = a(e^{-\tau/t_2} - e^{-\tau/t_1}) + b, \tag{3}$$

where t_1 and t_2 are, respectively, the rise and decay times of the signal. The constant b represents a very long-lived component of the signal with a lifetime exceeding the repetition period $T_L = 12.5$ ns of the laser pulses. This component results in a nonzero signal at negative delays. Exemplary fits are shown as smooth solid curves in the figure. The broadening increases with a characteristic time t_1 of about 40 ps and decays with

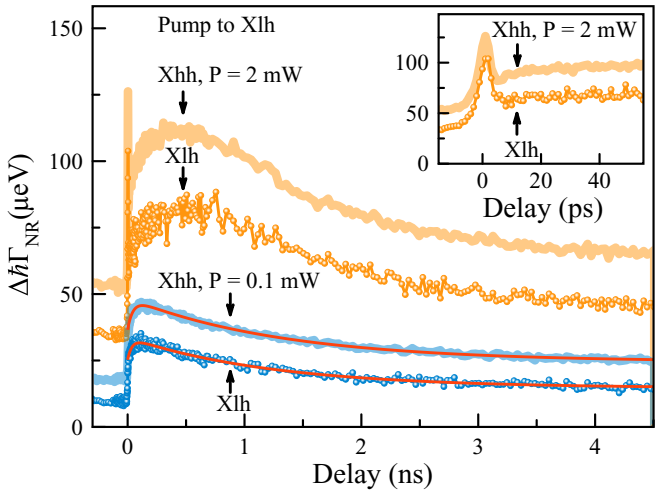

FIG. 4. Delay dependencies of the nonradiative broadening of the Xhh (solid lines) and Xlh (circles) resonances obtained with excitation to the Xlh transition with different excitation powers given in the legend. The background broadening not related to the excitation is subtracted. The smooth solid curves show the phenomenological fits of the Xhh and Xlh resonance broadenings by function (3) with characteristic times $t_1 \approx 40$ ps and $t_2 \approx 1300$ ps. Inset shows initial parts of the experimental dependencies. The sample temperature $T = 5$ K.

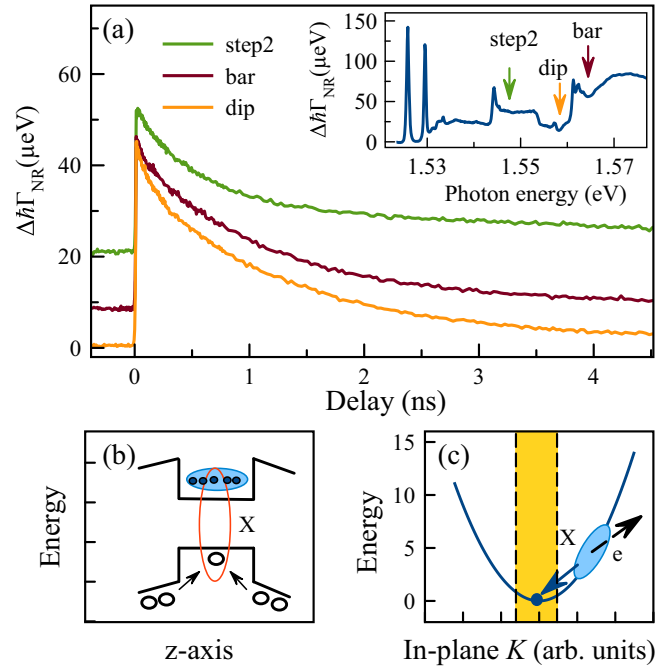

FIG. 5. (a) Comparison of the nonradiative broadening dynamics of the Xhh resonance obtained with excitation to different spectral points indicated by arrows in the inset. The background broadening not related to the optical excitation is subtracted. Excitation power $P = 0.2$ mW. (b) Illustration of the formation mechanism of charged excitons under excitation into the "dip" spectral region. (c) The mechanism of fast depletion of the nonradiative exciton reservoir via exciton scattering into the radiative Xhh state with a transfer of excess momentum to a free carrier.

a time t_2 of about 1.3 ns. This behavior of the broadening reflects the complex dynamics of excitons in the reservoir.

If the excitation power is relatively low, the light-induced broadening of the Xlh resonance is noticeably smaller than that of the Xhh one (see blue curves in Fig. 4). It becomes approximately twice smaller at large delays. Such behavior is consistent with the broadening of the resonances observed in the steady-state experiments (see Fig. 2 and the mechanism of the Xlh exciton broadening discussed in Sec. III).

The broadening of the Xhh and Xlh resonances rises sublinearly with the excitation power so that it is only about 2.5 times larger at $P_{\text{pump}} = 2$ mW compared to weak excitation $P_{\text{pump}} = 0.1$ mW. This sublinear behavior is consistent with the cw results (see Sec. III). The ratio of the Xhh to Xlh broadenings decreases with the excitation power, especially at small delays. This observation possibly points to an increase of the exciton reservoir temperature and, correspondingly, incomplete conversion of the photocreated light-hole excitons to heavy-hole ones. The broadening dynamics is more complex at strong excitation where the simple expression (3) stops to be a good approximation. We consider a more elaborate model for strong excitation in Sec. VI A.

In the case of excitation at higher energies up to the "dip" region, relatively small changes in the dynamics are observed. First, there is no rising part of the dynamics. Second, the broadenings of the Xhh and Xlh resonances come closer in magnitude in the initial part even at low excitation power. Eventually, in the case of excitation into the dip and the barrier, the broadening dynamics of the Xhh and Xlh resonances almost coincide.

Figure 5(a) shows the dynamics of the Xhh resonance broadening under excitation to several spectral points. The dynamics look similar, except for a drastic difference in the long-lived component. Excitation into the "step2" or barrier provides an accumulation of the reservoir excitons, so the broadening signal survives up to the next laser pulse. This component is seen as the background signal at negative delays.

When excited to the barrier layer with even higher energy, we observe similar dynamics. Such excitation, however, creates hot free electrons and holes in the barrier layers. They can travel within the heterostructure and participate in several processes, such as cooling and partial recombination of the carriers in the barrier layers, diffusion and capture into the QW layer, etc. While certainly an interesting topic, a detailed description of these processes is out of the scope of this paper.

In contrast to all other regimes, the excitation into the dip is not followed by an accumulation of excitons in the reservoir. There is no signal at a negative delay. As a result, the average broadening over the repetition period of laser pulses is considerably smaller than that for excitation to the "step2" or "bar" regions. This observation explains the dip in the NBE spectrum [see inset in Fig. 5(a)].

This feature of the dynamics points to an efficient mechanism of exciton reservoir depletion if the structure is excited into the dip region. This mechanism is definitely not linked to the nonradiative losses of excitons and carriers. Indeed, the PLE spectra in Fig. 3(a) demonstrate an *increase* of the PL intensity under excitation to this spectral region. So, we

conclude that the depletion comes from an efficient scattering of the reservoir excitons into the light cone followed by their radiative recombination.

According to the model of the energy structure discussed in the previous section, optical excitation into the dip creates one type of carrier in the QW and the other type in the barriers. The accuracy of material parameters for GaAs/AlGaAs heterostructures, such as the band offsets and the Luttinger parameters [47], is insufficient to draw a definite conclusion on the type of carriers that are first to delocalize in the barrier layers. We assume that holes delocalize before electrons so that excess electrons accumulate in the QW when the dip spectral region is excited [see Fig. 5(b)]. If a hole is captured into the QW, it couples with one of the electrons, forming an exciton in the nonradiative reservoir. However, many other electrons surround this exciton and it can be scattered into the light cone while its excess momentum is transferred to one of the free electrons. The scheme depicted in Fig. 5(c) shows this process.

In the framework of this model, the reservoir mainly consists of electrons rather than excitons. The electrons equally interact with the photocreated heavy-hole and light-hole excitons, which explains the equal broadening of the Xhh and Xlh resonances observed experimentally under excitation to the dip [see Fig. 2(a)]. If electrons were delocalized in the barriers first, the reservoir would contain excess holes. When holes cool down to the lattice temperature, they are converted to heavy holes. These holes can broaden the Xhh resonance via the exchange interaction but not the Xlh resonance. Therefore, an excess of holes must lead to larger broadening of the Xhh resonance compared to the Xlh resonance, which contradicts the experiment.

VI. MODEL OF THE EXCITON DYNAMICS

A. Excitation to the Xlh resonance

We assume that resonant excitation to the light-hole exciton state creates radiative excitons, which can either rapidly relax with the emission of photons or be scattered to the reservoir. The scattering of excitons into the reservoir can be caused by acoustic-phonon emission as well as by their interaction with each other or with the reservoir excitons and carriers. The approximation of the dynamic curves for a weak excitation shown in Fig. 4 gives a characteristic time of the transfer to the reservoir of about 40 ps. This time is about twice the radiative lifetime of the light-hole excitons. Consequently, only $\frac{1}{3}$ of the photocreated exciton population is scattered to the reservoir.

The excitons scattered to the reservoir can relax to the average reservoir temperature (fraction k of the "cold" excitons) or dissociate into electrons and holes [the $(1-k)$ fraction of the "hot" excitons]. This exciton dissociation process immediately explains the initial slow rise of the nonradiative broadening during several hundreds of picoseconds observed in the experiment for strong excitation (see Fig. 4). The dissociation rate is denoted as γ_d.

The last two processes, which we take into account, are the electron-hole coupling into excitons described by the rate κ_{ex} (the bimolecular process [39]) and the carrier-induced exciton scattering from the reservoir to the light cone characterized by the bimolecular rate constant κ_c. For simplicity, we do not explicitly consider any phonon-induced processes assuming that they can be taken into account by an appropriate choice of the model parameters. We also do not consider any contribution of the exciton-exciton interaction to the scattering of the excitons from the reservoir to the light cone. The presence of long-lived excitons in the reservoir indicates that this process should be less efficient than exciton-carrier scattering.

The system of kinetic equations describing the discussed processes is

$$\begin{aligned} n_x^{\mathrm{hot}} &= N_0(1-k)e^{-\gamma_d t}, \\ \frac{dn_{\mathrm{e}}}{dt} &= \gamma_d n_x^{\mathrm{hot}} - \kappa_{ex} n_{\mathrm{e}} n_{\mathrm{h}}, \\ \frac{dn_{\mathrm{h}}}{dt} &= \gamma_d n_x^{\mathrm{hot}} - \kappa_{ex} n_{\mathrm{e}} n_{\mathrm{h}}, \\ \frac{dn_x}{dt} &= \kappa_{ex} n_e n_h - \kappa_c n_x (n_{\mathrm{e}} + n_{\mathrm{h}}). \end{aligned} \tag{4}$$

Here, N_0 is the areal density of the excitons scattered to the reservoir; n_{e}, n_{h}, n_x, and n_x^{hot} are, respectively, the electron, hole, and "cold" and "hot" exciton densities in the reservoir. The initial conditions for these variables are $n_{\mathrm{e}}(0) = n_{\mathrm{h}}(0) = 0$, $n_x(0) = N_{bgr} + N_0 k$, where N_{bgr} is the background exciton density accumulated from the previous laser pulses.

This nonlinear system of equations has no analytical solution. We solved it numerically treating the constants N_0, k, γ_d, κ_{ex}, and κ_c as fitting parameters. The excitation-induced nonradiative broadening of the Xhh resonance is expressed via the carrier and exciton densities as follows:

$$\Delta\hbar\Gamma_{\mathrm{NR}} = \sigma_{\mathrm{eh}}(n_{\mathrm{e}} + n_{\mathrm{h}}) + \sigma_x\left(n_x^{\mathrm{hot}} + n_x\right). \tag{5}$$

Here, σ_{eh} and σ_x are the cross sections of the exciton-carrier (X-eh) and exciton-exciton (X-X) scatterings, respectively. The main mechanism of scattering of excitons and carriers at relatively small wave vectors is their exchange interaction (see Refs. [49,55,56]). The analysis performed in these works shows that the exchange constants for X-eh and X-X interactions in narrow QWs have similar values. For simplicity, we put $\sigma_{\mathrm{eh}} = \sigma_x \equiv \sigma$.

Examples of the theoretical curves obtained within this model are shown in Fig. 6. Thin solid lines show the dynamics of excitons and carriers in the reservoir at an excitation power of $P_{\mathrm{exc}} = 0.2$ mW. For an equal population of electrons and holes, the equations for the electrons and holes show the same dynamics [see Eqs. (4)], therefore, $n_{\mathrm{h}}(t) = n_{\mathrm{e}}(t)$. The modeling shows that the fraction of "cold" excitons is of about $k \approx 0.7$ at this excitation power. The dissociation rate parameter is $\gamma_d = 0.007\ \mathrm{ps}^{-1}$. The obtained values of the bimolecular rate constants are $\kappa_{ex} = 0.6\ \mu\mathrm{m}^2/\mathrm{ns}$ and $\kappa_c = 0.08\ \mu\mathrm{m}^2/\mathrm{ns}$. The values of κ_{ex} are of the same order of magnitude as those reported in Refs. [28,38,39]. The parameter κ_c is an order of magnitude smaller than κ_{ex}, which makes the carrier-induced scattering of reservoir excitons to the light cone the slowest process in our model.

To calibrate the exciton and carrier densities created in the reservoir by a single laser pulse, we have estimated the number of the photocreated excitons in the case of weak excitation with $P_{\mathrm{exc}} = 0.1$ mW. The number of photons that

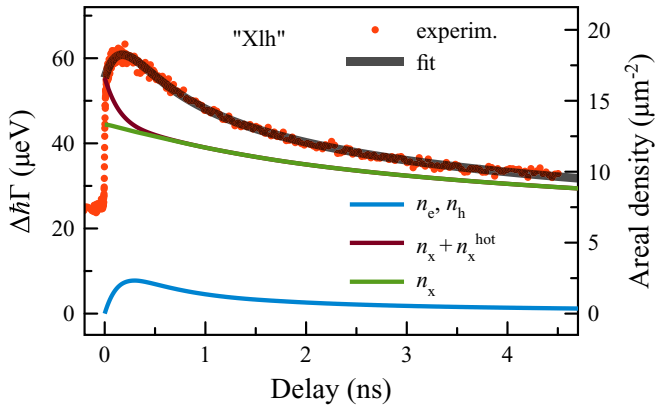

FIG. 6. Dynamics of the Xhh nonradiative broadening under excitation to the "Xlh" resonance (points, left vertical axis) and the model (thick solid curve). Thin solid curves show the dynamics of the carrier and exciton densities predicted by the model (right vertical axis). Excitation power $P = 0.2$ mW.

reach the QW layer from a single laser pulse at this power is $N_{\text{phot}} \approx 3 \times 10^6$. The absorption coefficient for an exciton transition is calculated using the standard formula [4]

$$a(\omega) = \frac{2\Gamma_R \Gamma_{NR}}{(\omega - \omega_X)^2 + (\Gamma_R + \Gamma_{NR})^2}.$$

Taking into account the values of the radiative broadening of the Xlh resonance $\hbar\Gamma_R \approx 15$ μeV, and its nonradiative broadening just before the pulse arrival $\hbar\Gamma_{NR} \approx 100$ μeV, we obtain the maximum value of $a(\omega_X) \approx 0.23$. We should also take into account that only 20% of the incident photons are absorbed because of the relatively large spectral width of the pump pulses (HWHM = 480 μeV) compared to that of the Xlh resonance [$\hbar(\Gamma_R + \Gamma_{NR}) = 115$ μeV] and also the presence of oscillating wings in the spectra of the pulses taking 18% of their energy. Accounting for the laser spot area on the sample, $S_{\text{spot}} \approx 7100$ μm^2, we obtain the areal density of the bright excitons created by a single laser pulse: $N_{\text{br}} = 20$ μm^{-2}. Approximately $\frac{1}{3}$ of the photocreated excitons end up in the reservoir. Therefore, the initial exciton density scattered to the reservoir is $N_0 \approx 7$ μm^{-2}. The obtained value of the exciton density allows us to estimate the cross section of the exciton-exciton scattering at this excitation power using expression (5): $\sigma_x \approx 3$ μeV μm^2.

B. Nonresonant excitation

The broadening dynamics of the Xhh resonance was experimentally measured for excitation to different spectral points above the Xlh exciton transition (see Sec. V). The excitation power was 0.2 mW.

The excitation to the "step1," "X3," and "step2" spectral regions creates mainly free carriers in the QW. We set $n_x^{\text{hot}} = 0$ in this case for simplicity. We also assume that the excitation creates hot electrons and holes, which only couple into excitons after they cool. The cooling process is considered to be exponential, $n_e^{\text{hot}} = n_h^{\text{hot}} = N_0 e^{-\gamma_T t}$, with a characteristic time $\tau_T = 1/\gamma_T = 100$ ps. The equations describing the dynamics

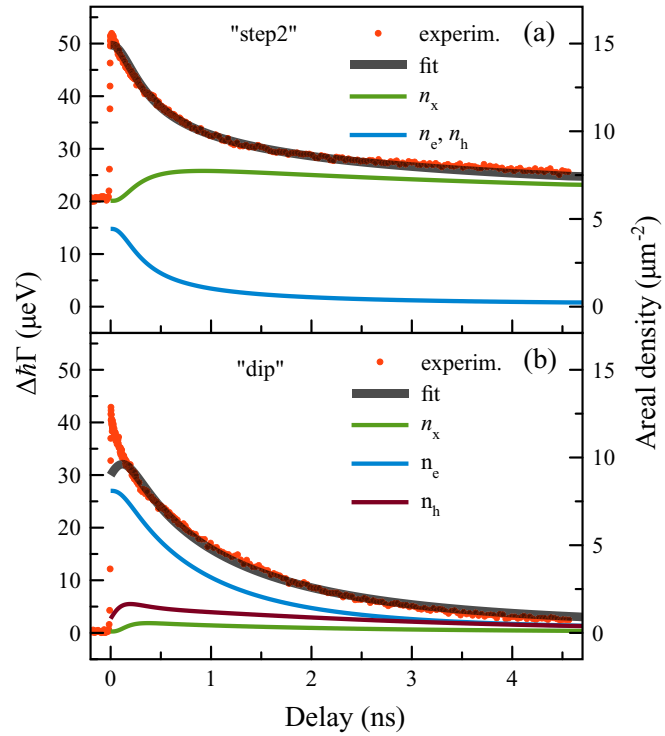

FIG. 7. (a) Dynamics of the Xhh nonradiative broadening for excitation to the "step2" region (points, left vertical axis) and its modeling (thick solid curve). The thin solid curves show the dynamics of the carrier and exciton densities (right vertical axis). Excitation power $P = 0.2$ mW. (b) The same for the case of the excitation to the dip spectral region.

of the exciton and carrier densities are

$$\begin{aligned}
\frac{dn_e}{dt} &= \gamma_T n_e^{\text{hot}} - \kappa_{ex} n_e n_h, \\
\frac{dn_h}{dt} &= \gamma_T n_h^{\text{hot}} - \kappa_{ex} n_e n_h, \\
\frac{dn_x}{dt} &= \kappa_{ex} n_e n_h - \kappa_c n_x (n_e + n_h).
\end{aligned} \tag{6}$$

The initial condition for the exciton and carrier densities $n_e(0) = n_h(0) = 0$, $n_x(0) = N_{bgr}$.

The fitting curve and the dynamics of the carrier and exciton densities obtained using Eqs. (6) are shown in Fig. 7(a). One can see that the theory reproduces the general behavior of the nonradiative broadening. The carrier density considerably decreases during the first nanosecond due to electrons and holes forming excitons. After the initial increase, the exciton density decays slowly with a single relevant relaxation process: scattering to the light cone by the free carriers. Since the carrier density is small at $t > 1$ ns, the scattering process is slow. We obtain the following values for the bimolecular rate constants: $\kappa_{ex} = 0.9$ μm^2/ns and $\kappa_c = 0.07$ μm^2/ns. These values are close to those obtained for weak excitation to the Xlh resonance.

The case of excitation to the dip spectral region requires particular attention. In this case, presumably, holes are created in the barrier layers while electrons accumulate in the QW layer. As a result, a charge imbalance appears in the QW. It

can persist for a long time, while the holes in the barriers relax to the QW layer. This process is illustrated in Fig. 5(b). Accordingly, the exciton reservoir can efficiently deplete. The rate equations describing these processes slightly differ from Eqs. (6):

$$\frac{dn_{\rm h}}{dt} = \gamma_b n_b + \gamma_T n_{\rm h}^{\rm hot} - \kappa_{ex} n_{\rm e} n_{\rm h},$$
$$\frac{dn_{\rm e}}{dt} = \gamma_T n_{\rm e}^{\rm hot} - \kappa_{ex} n_{\rm e} n_{\rm h},$$
$$\frac{dn_x}{dt} = \kappa_{ex} n_{\rm e} n_{\rm h} - \kappa_c n_x (n_{\rm e} + n_{\rm h}). \quad (7)$$

Here, $n_b = N_0(1-k)e^{-\gamma_b t}$, $n_{\rm e}^{\rm hot} = N_0 e^{-\gamma_T t}$, and $n_{\rm h}^{\rm hot} = kN_0 e^{-\gamma_T t}$. This system of equations follows under the assumption that the major part of holes [$(1-k) = 0.9$ in this case] is created in the barriers. The initial conditions for the exciton and carrier densities are $n_{\rm h}(0) = n_{\rm e}(0) = 0$, $n_x(0) = N_{bgr}$.

The modeled dynamics of the nonradiative broadening reproduces the experimentally observed dependence quite well [see Fig. 7(b)]. It only fails in the initial part of the curve at $t < 150$ ps.

The areal density of electrons in the QW is relatively large initially, $n_{\rm e}(0) + n_{\rm e}^{\rm hot}(0) = 8\ \mu{\rm m}^{-2}$, and slowly decays in time. The decay mainly comes from the capture of holes from the barriers (characteristic time $t_b = 1/\gamma_b = 770$ ps) followed by their coupling with the electrons. The bimolecular rate constant for the coupling $\kappa_{ex} = 0.77\ \mu{\rm m}^2/{\rm ns}$ is slightly larger than that for the case of the excitation to the Xlh resonance.

The scattering of the reservoir excitons to the light cone is very efficient in this case. This can be observed directly in the experimental data and finds confirmation in our model. The bimolecular rate constant for the exciton scattering is relatively large, $\kappa_c = 1.7\ \mu{\rm m}^2/{\rm ns}$, at least an order of magnitude larger than that for the case of the excitation to the Xlh resonance. This can be partially explained by the low effective temperature of electrons, which are created in the QW and have enough time for cooling.

We should mention that the experimentally observed dynamics of the exciton reservoir at stronger excitation (not shown here) becomes slower so that the nonzero broadening at the negative delay appears again. Such dynamics is characterized by a lower value of the rate κ_c.

VII. PL KINETICS

The model described in the previous section also predicts the time dependence of the PL signal. Indeed, the PL profile is given by the last term in the last equation of system (4),

$$I_{\rm PL}(t) = A_{\rm PL}\kappa_c n_x (n_{\rm e} + n_{\rm h}), \quad (8)$$

where $A_{\rm PL}$ is a scaling factor.

To verify the prediction of Eq. (8), we have measured the kinetics of the Xhh exciton PL for optical excitation at different energies. The kinetics were measured using a setup, which included a 2-ps tunable Ti:sapphire laser, a cryostat, a spectrometer, and a synchroscan streak camera. Examples of the PL kinetics are shown in Fig. 8. The top left panel shows a color map of the kinetics measured under excitation of the sample into the dip, $E_{\rm exc} = 1.5546$ eV. The two panels on the right show the cross sections of similar color maps at the energy of the Xhh exciton transition ($E_{\rm Xhh} = 1.5252$ eV) measured for excitation to the dip (the top panel) and to step2 (the bottom panel). We approximated the time dependencies of the PL by a phenomenological two-exponential function (3) with characteristic times t_1 and t_2. The bottom left panel depicts these times versus the excitation photon energy.

One can see that the PL signal lasts for at least 2 ns after the excitation pulse. This is orders of magnitude longer than the radiative lifetime of the Xhh exciton $\tau_{\rm Xhh} = 1/(2\Gamma_{\rm R}) \approx 10$ ps. Here we used the value of the radiative broadening $\hbar\Gamma_{\rm R} = 37\ \mu$eV (see Sec. II) and the well-known relation between the radiative time and $\Gamma_{\rm R}$ [4]. Hence, the PL kinetics are governed by the relaxation processes in the nonradiative reservoir discussed in the previous sections.

The model of the dynamic processes in the reservoir describes the PL pulse temporal profile reasonably well with no fitting parameters. This clearly indicates that all relevant processes are accounted for in the model. In particular, the PL signal decays almost to zero at $t > 2.5$ ns, which points to the free carriers as the origin of exciton scattering towards the light cone. We conclude that the contribution of the exciton-exciton and exciton-phonon scattering must be considerably smaller, otherwise we would expect to observe the tail of the PL for a duration on the scale of the reservoir lifetime, that is, until the next laser pulse.

Finally, we note that the PL data, similar to the dynamics of the Xhh broadening in the reflectivity spectra, show that the dip spectral region of the optical excitation takes a peculiar role. Indeed, as Fig. 8(c) shows, the PL decay time reaches the maximal value of t_2 if the structure is excited at this spectral region. This is intuitively consistent. The PL kinetics is governed by the free-carriers lifetime in the QW. When excited above or below the dip region, the free carriers are balanced within the QW. Their concentration rapidly decreases via formation of excitons. In this case, the PL decay time t_2 corresponds to the lifetime of the balanced carriers. In the case of excitation within the dip region, the lifetime of the unbalanced electrons increases since the recombination with holes happens only after they are captured from the barrier layers. The last process increases t_2, given that holes and excitons do not accumulate in the reservoir (see Fig. 7).

VIII. DISCUSSION

The model of dynamic processes in the reservoir discussed in Sec. VI quantitatively describes the dynamics of the nonradiative broadening of the Xhh resonance at different photon energies of excitation. The same model also predicts a PL pulse temporal profile, which is experimentally measurable. After solving the nonradiative broadening dynamics problem, the PL kinetics can be described using the same set of fit parameters.

There are several points in the model which, ideally, should be verified. To minimize the number of fitting parameters in the model we used one single universal constant σ, the cross section of the exciton-carrier and exciton-exciton scatterings

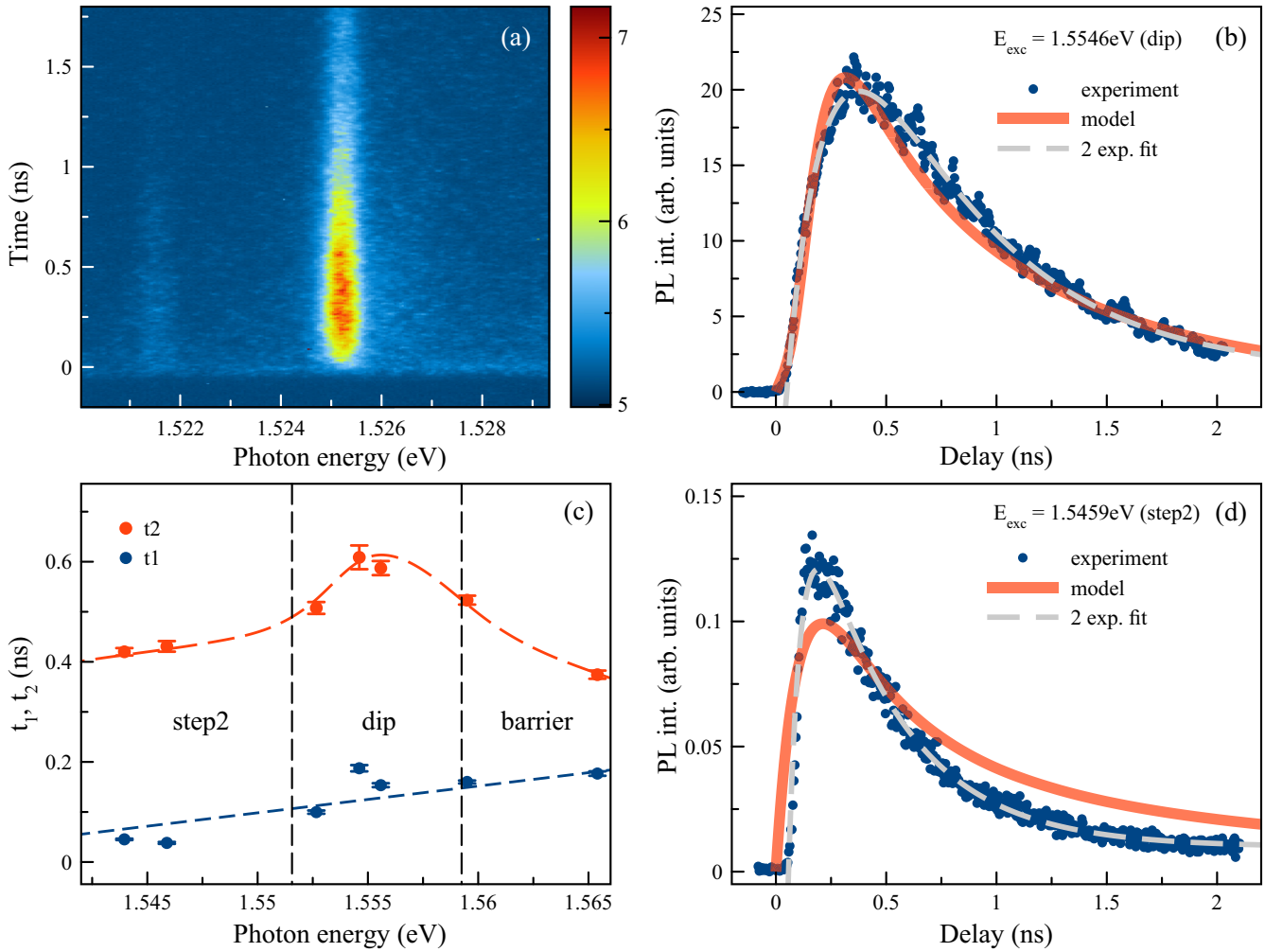

FIG. 8. (a) An example of the color plot of the PL kinetics in the spectral region around of the Xhh exciton measured at the excitation to the dip region ($E_{exc} = 1.5546$ eV). Excitation power $P_{exc} = 0.2$ mW; sample temperature $T = 8.3$ K. (b), (d) Show the cross sections of the color plots measured at the excitation to the dip (the upper panel) and step2 (the lower panel) regions. The dots are the experimental data. The dashed curves are the fits by function (3). The solid curves are the modeling by Eq. (8). (c) The rise and decay times of the PL kinetics obtained at the excitation to different spectral points. The blue dashed line is a linear approximation. The red dashed curve is a guide to the eye.

[see Eq. (5) and related text]. At the same time, the carriers created in the barrier layer under excitation to the dip or barrier spectral regions can acquire a large in-plane wave vector when they are captured in the QW layer. The exchange interaction of such carriers with excitons can be strongly affected, at least theoretically [49,55,56]. Such carriers still can efficiently broaden the exciton resonances, but they hardly scatter the reservoir excitons into the light cone.

Second, the exciton-exciton scattering, which we ignored, can contribute to the depletion of the nonradiative reservoir. Our experimental data in regimes when almost no free carriers are created (i.e., resonant excitation at low power in Fig. 4) shows that the Xhh nonradiative broadening decays in time. In other words, the exciton density in the reservoir decreases. Of course, this density decrease can be also caused by the exciton-phonon interaction [38,39]. It is desirable to include these processes in the model. However, to minimize the number of free parameters, the cross section of these processes should be evaluated for the structure under study.

The presence of the reservoir of nonradiative excitons can explain the rapid increase of the PL intensity just after the excitation pulse observed in many works (see, e.g., Refs. [25,27,28,30,34,36]). Indeed, the photocreated free carriers can scatter the nonradiative excitons accumulated from previous pulses into the light cone. An example of such a rapid increase of the PL is shown in Fig. 8(d). If the reservoir is empty, as in the case of excitation to the dip, the PL rise is relatively slow [see Fig. 8(b)].

Finally, we would like to point out that our results provide an alternative approach for an explanation of the rapid PL increase interpreted in terms of the resonant PL of a correlated electron-hole plasma in Ref. [40]. Our results show that the PL rise is naturally explained by the presence of real excitons in the nonradiative reservoir. A similar conclusion was achieved in Ref. [34].

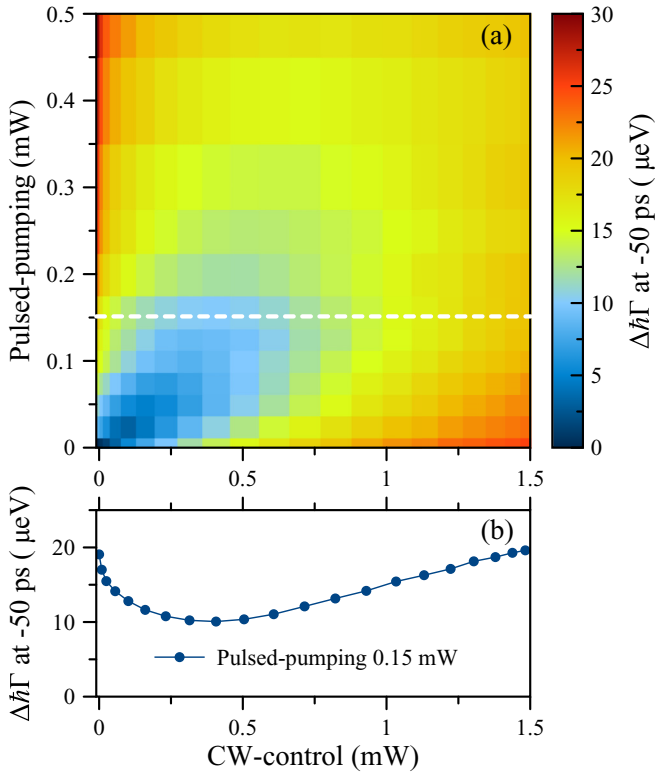

FIG. 9. (a) Color plot of the Xhh nonradiative broadening measured at small negative delays. The "cw control" is adjusted to the dip spectral region and the pulsed pump to the Xlh resonance. (b) Shows cross section of (a) along the white dashed line.

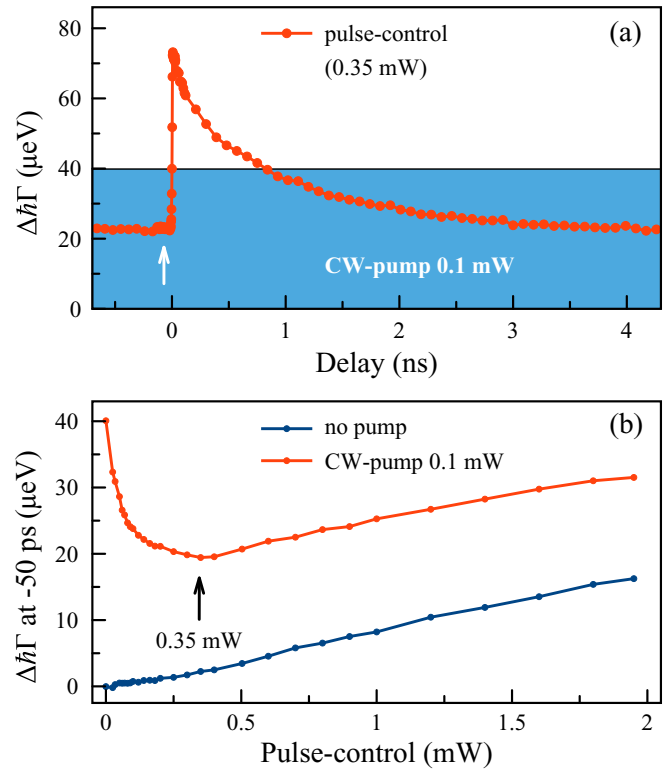

FIG. 10. (a). Dynamics of the Xhh nonradiative broadening under "cw pump" to the Xlh resonance ($P_{cw} = 0.1$ mW) and "pulsed control" ($P_{pulse} = 0.35$ mW) to the dip spectral region. Blue area indicates the broadening without the pulsed control. (b) The pulsed-control power dependence of the Xhh nonradiative broadening measured at the negative delay in the presence of cw pump (red curve) and with no cw pump (blue curve).

IX. CONTROL OF EXCITON RESERVOIR

Our results show that, in high-quality QWs, the main mechanism of depleting the exciton reservoir is related to the exciton-free carrier scattering. This fact opens up an opportunity to control the exciton reservoir. We can populate the reservoir with excitons or depopulate it with uncompensated free carriers. A proper choice of the excitation photon energy provides either of these options. Besides, we can read out the state of the reservoir experimentally. The reservoir state with large free-carrier concentration will be depleted efficiently, which in turn results in a smaller nonradiative broadening of exciton resonances. Accordingly, when switching the state of the reservoir by additional excitation, we may directly observe the modified nature of the carriers in the reservoir via exciton broadening.

We implemented this idea in two ways using two available lasers, a pulsed and a cw laser, respectively. First, we use the laser pulses to create excitons in the reservoir via excitation to the Xlh resonance. In the following, we will call this excitation scheme "pulsed pumping." We monitor the areal density of excitons in the reservoir by measuring the nonradiative broadening of the Xhh exciton resonance at negative delays between the pump and probe pulses. The cw laser beam called "cw control" is used to create free carriers in the reservoir via excitation to the dip spectral region. Figure 9(a) shows a 2D map of the broadening versus the excitation powers of the two lasers. As seen, the cw control indeed renders it possible to deplete the exciton reservoir partially. An exemplaric cross section of the 2D plot for a pulsed pump power of 150 μW is shown in Fig. 9(b). It demonstrates a twofold decrease of the nonradiative broadening and, correspondingly, of the exciton areal density in the reservoir at the optimal cw-control power of about 0.4 mW at this pump power.

Second, we use the opposite experimental configuration when the cw pump creates the exciton reservoir via excitation to the Xlh resonance and the pulsed control creates the unbalanced free carriers via excitation to the dip spectral region. As seen in Fig. 10(a), the cw pump alone with power of 0.1 mW creates the exciton reservoir, which additionally broadens the Xhh resonance by about 40 μeV (blue area in this figure). When the pulsed control is switched on, the dynamics of the nonradiative broadening demonstrate an intense peak during the first one nanosecond [see the red curve in Fig. 10(a)]. As discussed above (Sec. VI), this peak appears due to the creation of the free carriers. At larger delays, the broadening becomes *smaller* than that in the absence of the pulsed control. This is a clear indication of depleting the exciton reservoir by free carriers created by the pulsed control. Figure 10(b) in this figure illustrates the power dependence of the nonradiative broadening at the negative delay. Without the cw pump, the broadening and, correspondingly, the exciton density in the reservoir is relatively small (see blue curve). The red curve clearly shows the effect of depopulation of the exciton

reservoir created by the cw pump. Similar to Fig. 9(b), a twofold decrease of the nonradiative broadening is observed when the pulsed control is switched on with some optimal power of about 0.35 mW.

X. CONCLUSION

In this work, we experimentally studied the dynamics of nonradiative excitons with large in-plane K vectors in a high-quality structure containing a shallow QW. Our method is based on the detection of the nonradiative broadening of exciton resonances induced by scattering of bright excitons on an optically created mixture of reservoir excitons and free carriers. We introduced the NBE spectrum, which represents the broadening of a certain spectral line as a function of the cw excitation energy. This kind of spectrum provides unique insights into the population of excitons in a reservoir created by resonant and nonresonant excitation. Using a nondegenerate spectrally resolved pump-probe technique, we studied the dynamics of nonradiative excitons under pulsed excitation to several relevant spectral regions which results in different carrier generation regimes. If during the excitation process excitons and free carriers are created predominantly inside the QW layer, the dynamics consists of a fast decay of the nonradiative broadening of the Xhh and Xlh resonances followed by a long-lived "tail," surviving up to the next laser pulse. This points to the accumulation of nonradiative excitons in the reservoir.

We proposed a kinetic model describing the dynamics of nonradiative excitons. To minimize the number of free parameters, we considered very few dynamic processes in the reservoir. Namely, the association of carriers into excitons and the scattering of excitons to the light cone are considered in the cases where the optical excitation created free carriers in the QW layer. In the case of excitation into exciton resonances, the scattering of excitons to the reservoir and their dissociation are also taken into account. At higher excitation photon energy, the creation of carriers in the barrier layers becomes possible as well and we consider their subsequent capture into the QW layer. The model well describes the exciton dynamics observed experimentally. The obtained values of the bimolecular coupling rate are close to those reported in the literature. The model was capable to reproduce the experimental temporal profiles of the PL pulses without fitting parameters.

An important feature of the studied sample is the presence of a spectral area slightly below the bandgap of barrier layers, we called "dip," in which optical transitions correspond to creating electrons in the QW layer and delocalized holes in the barrier layers. Optical excitation into this region produces an imbalance of carriers in the QW layer which changes the dynamics of nonradiative excitons in the reservoir drastically, provoking its depletion. This phenomenon is also well described by our model, which considers the exciton-free-carrier scattering as the main mechanism of the reservoir population decay and the PL formation. The controlled preparation of a carrier imbalance in the nonradiative reservoir of exciton-free-carrier mixtures paves the way to control the exciton reservoir population without bleaching of PL intensity. In our experiments, pulsed and cw excitation into the dip spectral region allowed us to reduce the population in the reservoir created by resonant excitation of excitons by a factor of 2. Potentially, this effect can improve the capabilities of optical traps for polaritons in microcavity heterostructures [57–63] giving rise to independent control of the magnitude of potential landscapes and polariton pumping. The methods of characterization and optical control of the reservoir of dark excitons developed here can be employed in a wide range of semiconductor structures. High-quality GaAs quantum wells studied here served as a test bed for the optimization of the experimental technique.

ACKNOWLEDGMENTS

The authors acknowledge financial support by the Deutsche Forschungsgemeinschaft through the International Collaborative Research Centre TRR 160, Grant No. 249492093 (project B7), Russian Foundation for Basic Research, Grants No. 19-52-12032 and No. 19-02-00576, and SPbU, Grant No. 73031758. The authors thank Recourse Center "Nanophotonics" SPbU for the heterostructure studied in this work. The authors thank the developers of the MAGICPLOT software, which was used to analyze a large amount of experimental data. A.S.K and A.V.T acknowledge RFBR Grant No. 20-32-70131. A.V.K. acknowledges the support by the Westlake University (Project No. 041020100118).

[1] E. F. Gross and N. A. Karryjew, The optical spectrum of the exciton, Dokl. Akad. Nauk SSSR **84**, 471 (1952).

[2] J. J. Hopfield, Theory of the contribution of excitons to the complex dielectric constant of crystals, Phys. Rev. **112**, 1555 (1958).

[3] B. Deveaud, F. Clérot, N. Roy, K. Satzke, B. Sermage, and D. S. Katzer, Enhanced Radiative Recombination of Free Excitons in GaAs Quantum Wells, Phys. Rev. Lett. **67**, 2355 (1991).

[4] E. L. Ivchenko, *Optical Spectroscopy of Semiconductor Nanostructures* (Springer, Berlin, 2004).

[5] L. V. Butov, C. W. Lai, A. L. Ivanov, A. C. Gossard, and D. S. Chemla, Towards Bose–Einstein condensation of excitons in potential traps, Nature (London) **417**, 47 (2002).

[6] P. G. Lagoudakis, M. D. Martin, J. J. Baumberg, A. Qarry, E. Cohen, and L. N. Pfeiffer, Electron-Polariton Scattering in Semiconductor Microcavities, Phys. Rev. Lett. **90**, 206401 (2003).

[7] M. Wouters, T. K. Paraïso, Y. Léger, R. Cerna, F. Morier-Genoud, M. T. Portella-Oberli, and B. Deveaud-Plédran, Influence of a nonradiative reservoir on polariton spin multistability, Phys. Rev. B **87**, 045303 (2013).

[8] N. Takemura, M. D. Anderson, S. Trebaol, S. Biswas, D. Y. Oberli, M. T. Portella-Oberli, and B. Deveaud, Dephasing effects on coherent exciton-polaritons and the breakdown of the strong coupling regime, Phys. Rev. B **92**, 235305 (2015).

[9] A. V. Kavokin, J. J. Baumberg, G. Malpuech, and F. P. Laussy, *Microcavities* (Oxford University, New York, 2017).

[10] D. Schmidt, B. Berger, M. Kahlert, M. Bayer, C. Schneider, S. Höfling, E. S. Sedov, A. V. Kavokin, and M. Aßmann, Tracking Dark Excitons with Exciton Polaritons in Semiconductor Microcavities, Phys. Rev. Lett. **122**, 047403 (2019).

[11] B. Berger, D. Schmidt, X. Ma, S. Schumacher, C. Schneider, S. Höfling, and M. Aßmann, Formation dynamics of exciton-polariton vortices created by nonresonant annular pumping, Phys. Rev. B **101**, 245309 (2020).

[12] L. C. Andreani, F. Tassone, and F. Bassani, Radiative lifetime of free excitons in quantum wells, Solid State Commun. **77**, 641 (1991).

[13] E. S. Khramtsov, P. A. Belov, P. S. Grigoryev, I. V. Ignatiev, S. Yu. Verbin, Yu. P. Efimov, S. A. Eliseev, V. A. Lovtcius, V. V. Petrov, and S. L. Yakovlev, Radiative decay rate of excitons in square quantum wells: Microscopic modeling and experiment, J. Appl. Phys. **119**, 184301 (2016).

[14] T. C. Damen, J. Shah, D. Y. Oberli, D. S. Chemla, J. E. Cunningham, and J. M. Kuo, Dynamics of exciton formation and relaxation in GaAs quantum wells, Phys. Rev. B **42**, 7434 (1990).

[15] A. V. Trifonov, E. S. Khramtsov, K. V. Kavokin, I. V. Ignatiev, A. V. Kavokin, Y. P. Efimov, S. A. Eliseev, P. Yu. Shapochkin, and M. Bayer, Phys. Rev. Lett. **122**, 147401 (2019).

[16] B. N. Murdin, W. Heiss, C. J. G. M. Langerak, S.-C. Lee, I. Galbraith, G. Strasser, E. Gornik, M. Helm, and C. R. Pidgeon, Direct observation of the LO phonon bottleneck in wide GaAs/$Al_xGa_{1-x}As$ quantum wells, Phys. Rev. B **55**, 5171 (1997).

[17] A. J. Nozik, Spectroscopy and hot electron relaxation dynamics in semiconductor quantum wells and quantum dots, Annu. Rev. Phys. Chem. **52**, 193 (2001).

[18] A. V. Trifonov, S. N. Korotan, A. S. Kurdyubov, I. Ya. Gerlovin, I. V. Ignatiev, Yu. P. Efimov, S. A. Eliseev, V. V. Petrov, Yu. K. Dolgikh, V. V. Ovsyankin, and A. V. Kavokin, Nontrivial relaxation dynamics of excitons in high-quality InGaAs/GaAs quantum wells, Phys. Rev. B **91**, 115307 (2015).

[19] S. Sim, H.-S. Shin, D. Lee, J. Lee, M. Cha, K. Lee, and H. Choi, Opposite behavior of ultrafast dynamics of exciton shift and linewidth broadening in bilayer ReS_2, Phys. Rev. B **103**, 014309 (2021).

[20] H. M. Gibbs, G. Khitrova, and S. W. Koch, Exciton-polariton light-semiconductor coupling effects, Nat. Photonics **5**, 273 (2011).

[21] S. Bieker, T. Henn, T. Kiessling, W. Ossau, and L. W. Molenkamp, Spatially Resolved Thermodynamics of the Partially Ionized Exciton Gas in GaAs, Phys. Rev. Lett. **114**, 227402 (2015).

[22] R. Eccleston, R. Strobel, W. W. Rühle, J. Kuhl, B. F. Feuerbacher, and K. Ploog, Exciton dynamics in a GaAs quantum well, Phys. Rev. B **44**, 1395(R) (1991).

[23] H. W. Yoon, D. R. Wake, and J. P. Wolfe, Effect of exciton-carrier thermodynamics on the GaAs quantum well photoluminescence, Phys. Rev. B **54**, 2763 (1996).

[24] M. Gurioli, P. Borri, M. Colocci, M. Gulia, F. Rossi, E. Molinari, P. E. Selbmann, and P. Lugli, Exciton formation and relaxation in GaAs epilayers, Phys. Rev. B **58**, R13403(R) (1998).

[25] J. Szczytko, L. Kappei, J. Berney, F. Morier-Genoud, M. T. Portella-Oberli, and B. Deveaud, Determination of the Exciton Formation in Quantum Wells from Time-Resolved Interband Luminescence, Phys. Rev. Lett. **93**, 137401 (2004).

[26] S. Chatterjee, C. Ell, S. Mosor, G. Khitrova, H. M. Gibbs, W. Hoyer, M. Kira, S. W. Koch, J. P. Prineas, and H. Stolz, Excitonic Photoluminescence in Semiconductor Quantum Wells: Plasma versus Excitons, Phys. Rev. Lett. **92**, 067402 (2004).

[27] J. Szczytko, L. Kappei, J. Berney, F. Morier-Genoud, M. T. Portella-Oberli, and B. Deveaud, Origin of excitonic luminescence in quantum wells: Direct comparison of the exciton population and Coulomb correlated plasma models, Phys. Rev. B **71**, 195313 (2005).

[28] B. Deveaud, L. Kappei, J. Berney, F. Morier-Genoud, M. T. Portella-Oberli, J. Szczytko, and C. Piermarocchi, Excitonic effects in the luminescence of quantum wells, Chem. Phys. **318**, 104 (2005).

[29] M. Nakayama, T. Ohno, and Y. Furukawa, Systematic investigation of effects of exciton-acoustic-phonon scattering on photoluminescence rise times of free excitons in GaAs/$Al_{0.3}Ga_{0.7}As$ single quantum wells, J. Appl. Phys. **117**, 134306 (2015).

[30] M. Beck, J. Hübner, M. Oestreich, S. Bieker, T. Henn, T. Kiessling, W. Ossau, and L. W. Molenkamp, Thermodynamic origin of the slow free exciton photoluminescence rise in GaAs, Phys. Rev. B **93**, 081204(R) (2016).

[31] J. Cerne, J. Kono, M. S. Sherwin, M. Sundaram, A. C. Gossard, and G. E. W. Bauer, Terahertz Dynamics of Excitons in GaAs/AlGaAs Quantum Wells, Phys. Rev. Lett. **77**, 1131 (1996).

[32] R. A. Kaindl, M. A. Carnahan, D. Hägele, R. Lövenich, and D. S. Chemla, Ultrafast terahertz probes of transient conducting and insulating phases in an electron-hole gas, Nature (London) **423**, 734 (2003).

[33] I. Galbraith, R. Chari, S. Pellegrini, P. J. Phillips, C. J. Dent, A. F. G. van der Meer, D. G. Clarke, A. K. Kar, G. S. Buller, C. R. Pidgeon, B. N. Murdin, J. Allam, and G. Strasser, Excitonic signatures in the photoluminescence and terahertz absorption of a GaAs/$Al_xGa_{1-x}As$ multiple quantum well, Phys. Rev. B **71**, 073302 (2005).

[34] R. A. Kaindl, D. Hägele, M. A. Carnahan, and D. S. Chemla, Transient terahertz spectroscopy of excitons and unbound carriers in quasi-two-dimensional electron-hole gases, Phys. Rev. B **79**, 045320 (2009).

[35] R. Ulbricht, E. Hendry, T. F. Heinz, and M. Bonn, Carrier dynamics in semiconductors studied with time-resolved terahertz spectroscopy, Rev. Mod. Phys. **83**, 543 (2011).

[36] S. Zybell, J. Bhattacharyya, S. Winnerl, F. Esser, M. Helm, H. Schneider, L. Schneebeli, C. N. Böttge, M. Kira, S. W. Koch, A. M. Andrews, and G. Strasser, Characterizing intra-exciton Coulomb scattering in terahertz excitations, Appl. Phys. Lett. **105**, 201109 (2014).

[37] X. Li, K. Yoshioka, Q. Zhang, N. M. Peraca, F. Katsutani, W. Gao, G. T. Noe II, J. D. Watson, M. J. Manfra, I. Katayama, J. Takeda, and J. Kono, Observation of Photoinduced Terahertz Gain in GaAs Quantum Wells: Evidence for Radiative Two-Exciton-to-Biexciton Scattering, Phys. Rev. Lett. **125**, 167401 (2020).

[38] C. Piermarocchi, F. Tassone, V. Savona, and A. Quattropani, Nonequilibrium dynamics of free quantum-well excitons in time-resolved photoluminescence, Phys. Rev. B **53**, 15834 (1996).

[39] C. Piermarocchi, F. Tassone, V. Savona, and A. Quattropani, Exciton formation rates in GaAs/$Al_xGa_{1-x}As$ quantum wells, Phys. Rev. B **55**, 1333 (1997).

[40] M. Kira, F. Jahnke, and S. W. Koch, Microscopic Theory of Excitonic Signatures in Semiconductor Photoluminescence, Phys. Rev. Lett. **81**, 3263 (1998).

[41] M. Kira and S. W. Koch, Many-body correlations and excitonic effects in semiconductor, Prog. Quantum Electron. **30**, 155 (2006).

[42] S. W. Koch, M. Kira, G. Khitrova, and H. M. Gibbs, Semiconductor excitons in new light, Nat. Mater. **5**, 523 (2006).

[43] A. V. Trifonov, I. V. Ignatiev, K. V. Kavokin, A. V. Kavokin, P. Yu. Shapochkin, Yu. P. Efimov, S. A. Eliseev, and V. A. Lovtcius, On the suppression of electron-hole exchange interaction in a reservoir of nonradiative excitons, Semiconductors **53**, 1170 (2019).

[44] P. Yu. Shapochkin, S. A. Eliseev, V. A. Lovtcius, Yu. P. Efimov, P. S. Grigoryev, E. S. Khramtsov, and I. V. Ignatiev, Excitonic Probe for Quantum-State Engineering by MBE Technology, Phys. Rev. Appl. **12**, 034034 (2019).

[45] E. S. Khramtsov, P. S. Grigoryev, D. K. Loginov, I. V. Ignatiev, Yu. P. Efimov, S. A. Eliseev, P. Yu. Shapochkin, E. L. Ivchenko, and M. Bayer, Exciton spectroscopy of optical reflection from wide quantum wells, Phys. Rev. B **99**, 035431 (2019).

[46] P. S. Grigoryev, A. S. Kurdyubov, M. S. Kuznetsova, I. V. Ignatiev, Yu. P. Efimov, S. A. Eliseev, V. V. Petrov, V. A. Lovtcius, and P. Yu. Shapochkin, Excitons in asymmetric quantum wells, Superlattices Microstruct. **97**, 452 (2016).

[47] I. Vurgaftman, J. R. Meyer, and L. R. Ram-Mohan, Band parameters for III–V compound semiconductors and their alloys, J. Appl. Phys. **89**, 5815 (2001).

[48] P. K. Basu and P. Ray, Energy relaxation of hot two-dimensional excitons in a GaAs quantum well by exciton-phonon interaction, Phys. Rev. B **45**, 1907 (1992).

[49] C. Ciuti, V. Savona, C. Piermarocchi, A. Quattropani, and P. Schwendimann, Role of the exchange of carriers in elastic exciton-exciton scattering in quantum wells, Phys. Rev. B **58**, 7926 (1998).

[50] D. F. Mursalimov, A. V. Mikhailov, A. S. Kurdyubov, A. V. Trifonov, and I. V. Ignatiev, Nontrivial dependence of spectral characteristics of excitons in quantum wells on the power of the resonant optical excitation, Semiconductors (to be published).

[51] J. H. Davies, *The Physics of Low-dimensional Semiconductors: An Introduction* (Cambridge University Press, Cambridge, 1998).

[52] R. C. Miller, A. C. Gossard, G. D. Sanders, Y.-C. Chang, and J. N. Schulman, New evidence of extensive valence-band mixing in GaAs quantum wells through excitation photoluminescence studies, Phys. Rev. B **32**, 8452 (1985).

[53] E. L. Ivchenko, A. Yu. Kaminski, and U. Rössler, Heavy-light hole mixing at zinc-blende (001) interfaces under normal incidence, Phys. Rev. B **54**, 5852 (1996).

[54] R. Magri and A. Zunger, Anticrossing and coupling of light-hole and heavy-hole states in (001) GaAs/$Al_xGa_{1-x}As$ heterostructures, Phys. Rev. B **62**, 10364 (2000).

[55] G. Ramon, A. Mann, and E. Cohen, Theory of neutral and charged exciton scattering with electrons in semiconductor quantum wells, Phys. Rev. B **67**, 045323 (2003).

[56] H. Ouerdane, R. Varache, M. E. Portnoi, and I. Galbraith, Photon emission induced by elastic exciton-carrier scattering in semiconductor quantum wells, Eur. Phys. J. B **65**, 195 (2008).

[57] G. Tosi, G. Christmann, N. Berloff, P. Tsotsis, T. Gao, Z. Hatzopoulos, P. G. Savvidis, and J. J. Baumberg, Sculpting oscillators with light within a nonlinear quantum fluid, Nat. Phys. **8**, 190 (2012).

[58] P. Cristofolini, A. Dreismann, G. Christmann, G. Franchetti, N. G. Berloff, P. Tsotsis, Z. Hatzopoulos, P. G. Savvidis, and J. J. Baumberg, Optical Superfluid Phase Transitions and Trapping of Polariton Condensates, Phys. Rev. Lett. **110**, 186403 (2013).

[59] A. Askitopoulos, H. Ohadi, A. V. Kavokin, Z. Hatzopoulos, P. G. Savvidis, and P. G. Lagoudakis, Polariton condensation in an optically induced two-dimensional potential, Phys. Rev. B **88**, 041308(R) (2013).

[60] R. Dall, M. D. Fraser, A. S. Desyatnikov, G. Li, S. Brodbeck, M. Kamp, C. Schneider, S. Höfling, and E. A. Ostrovskaya, Creation of Orbital Angular Momentum States with Chiral Polaritonic Lenses, Phys. Rev. Lett. **113**, 200404 (2014).

[61] S. Alyatkin, J. D. Töpfer, A. Askitopoulos, H. Sigurdsson, and P. G. Lagoudakis, Optical Control of Couplings in Polariton Condensate Lattices, Phys. Rev. Lett. **124**, 207402 (2020).

[62] J. Schmutzler, P. Lewandowski, M. Aßmann, D. Niemietz, S. Schumacher, M. Kamp, C. Schneider, S. Höfling, and M. Bayer, All-optical flow control of a polariton condensate using nonresonant excitation, Phys. Rev. B **91**, 195308 (2015).

[63] D. Niemietz, J. Schmutzler, P. Lewandowski, K. Winkler, M. Aßmann, S. Schumacher, S. Brodbeck, M. Kamp, C. Schneider, S. Höfling, and M. Bayer, Experimental realization of a polariton beam amplifier, Phys. Rev. B **93**, 235301 (2016).